Enhanced corrosion inhibition of copper in acidic environment by cathodic control of interface formation with 2-mercaptobenzothiazole

Vishant Garg, Sagar B Sharma, Sandrine Zanna, Antoine Seyeux, Frédéric Wiame, Vincent Maurice, Philippe Marcus

Author preprint published in *Electrochimica Acta*
https://doi.org/10.1016/j.electacta.2023.142162

Enhanced corrosion inhibition of copper in acidic environment by cathodic control of interface formation with 2-mercaptobenzothiazole

Vishant Garg, Sagar B. Sharma, Sandrine Zanna, Antoine Seyeux,
Frédéric Wiame, Vincent Maurice[1], Philippe Marcus[2]

PSL University, CNRS – Chimie ParisTech, Institut de Recherche de Chimie Paris,
Physical Chemistry of Surfaces Research Group,
11 rue Pierre et Marie Curie, 75005 Paris, France.

[1] Corresponding author for the work: vincent.maurice@chimieparistech.psl.eu
[2] Corresponding author for the work: philippe.marcus@chimieparistech.psl.eu

Abstract

Electrochemistry along with advanced surface analyses (X-ray photoelectron spectroscopy and time-of-flight secondary ion mass spectrometry) were implemented to investigate copper corrosion inhibition by 2-mercaptobenzothiazole (2-MBT) in hydrochloric aqueous solution and the effects of electrochemical control on the formation of the inhibiting interface. It is shown that reducing the native surface oxide by cathodic reduction prior to exposure to the inhibitor drastically decreases the rate of anodic dissolution. Additionally, increasing the exposure time of the metal surface to the inhibitor results in even better protection against dissolution. 2-MBT adsorbs as multilayers and bonds to both metallic copper and residual copper oxide islands via its sulphur atoms. Partial dissociation of the molecule, releasing the exocyclic sulphur, which then bonds to metallic Cu, is observed. Further dissociation of the molecule, releasing the endocyclic sulphur, is induced by anodic polarization, forming defects in the organic layer and thus compromising the barrier properties of the organic layer.

Keywords

Corrosion Inhibition; Copper; Cyclic Voltammetry; XPS; ToF-SIMS

1. Introduction

Copper is a widely used metal due to its excellent thermal and electrical conductivity. It is corrosion resistant in atmospheric conditions owing to a passive oxide layer, naturally forming on the surface, which provides protection against corrosive attack [1]–[3]. However, passivity is only maintained in slightly acidic, neutral, and alkaline conditions (pH>5), as predicted by the Pourbaix diagram [4]. In more strongly acidic conditions (pH<5), the passive oxide layer dissolves easily, leaving the metal unprotected [5], [6]. Additionally, the presence of chlorine ions in the environment can have a detrimental effect on the corrosion resistance of the metal since it tends to poison the formation of the protective passive oxide layer by competitively adsorbing chlorine on the metal and forming a $CuCl_2^-$ species that can dissolve instead of stabilizing the surface [7]–[10].

Among organic molecules [11]–[17], 2-mercaptobenzothiazole (2-MBT) is a well-known inhibitor that has been shown to efficiently protect metals such as copper, aluminium alloys, and stainless steels from corrosive attack [18]–[20]. Its chemical formula is $C_7H_5NS_2$, with a benzene ring (C_6H_4) bonded to 1 S and 1 N endocyclic atoms, forming another cycle with an additional C atom. The C atom in the second ring is bonded to an exocyclic S atom. Depending on the conformer of the molecule, the last H atom is bonded to either the endocyclic nitrogen or the exocyclic sulphur atom in the molecule [21], [22]. The S and N heteroatoms with high electron density are active sites that can coordinatively bond with metal atoms, enabling the molecule to strongly adsorb and to form a dense and protective film on the surface of the metal [20], [22]–[28].

There have been several experimental works addressing the bonding mechanisms of 2-MBT with copper surfaces, including the role of the sulphur and nitrogen atoms. Some authors concluded that the interaction between the molecule and the metal surface occurs via both sulphur atoms of the molecule [24], while others reported that it was only via the exocyclic sulphur atom [27]. Additionally, the involvement of the nitrogen atom along with the exocyclic sulphur has also been proposed [22], [25]. Density functional theory (DFT) modelling has shown that, depending on the thione or thiolate conformer of the molecule, the bonding of the 2-MBT molecule differs with the metallic or oxidized copper surface. In the thione form, there would be two modes of adsorption for 2-MBT, both in an upright configuration via its S

atoms covalently bonded to metallic Cu or via its exocyclic S atom bonded to oxidized Cu and H-bonding between the NH group and surface oxygen. In the thiolate form, the N and exocyclic S atoms would covalently bond to the surface also in an upright configuration [29], [30]. Therefore, the precise mechanism of bonding remains to be determined experimentally, although it is well-established from modelling studies that 2-MBT can strongly bonds to copper and form a protective barrier layer on the surface [29]–[31].

Controlling the metallic or oxidized state of the surface is a prerequisite to a better understanding of the bonding mechanisms of the molecule. In a work where the interface was prepared and controlled under ultra-high vacuum with deposition of the molecule from the vapour phase in ultra-low pressure conditions, it was shown that 2-MBT adsorbs on oxide-free metallic copper surfaces as well as on oxidized copper surfaces by its two sulphur atoms along with some free sulphur atoms dissociated from the molecule [24]–[26], [32], and that increasing the exposure to the molecule results in the build-up of multilayers of the organic film, in agreement with previous work with DFT modelling on metallic copper [30]. In neutral aqueous solution, it was also determined that the bonding between the 2-MBT molecule and the native oxide-covered copper surface occurred via the two sulphur atoms, forming multilayers of the organic film, and inhibiting further oxide growth [28].

The adsorption mechanisms of the 2-MBT molecule from an aqueous solution can also be altered by other factors such as the presence of residual native oxides, the nature of the electrolyte and its pH, the inhibitor concentration, and the presence of impurities or aggressive species. Therefore, it is not only imperative to study the adsorption of 2-MBT on copper and the protection offered by it in different environments, but methods of controlling the interface between the substrate and the inhibitor layer must be adapted to improve our understanding of the inhibition properties and eventually optimize the protection efficiency of the organic barrier layer.

In the present work, the adsorption and corrosion inhibition of 2-MBT on copper were studied in a hydrochloric acidic medium in which copper does not passivate. The formation of the inhibitive layer was controlled by applying different cathodic pre-treatment methods in the presence or absence of the inhibitor in the solution. Cyclic voltammetry (CV) was applied to determine the protection offered by the 2-MBT organic inhibitor layer against the anodic dissolution of copper. Electrochemistry along with surface analysis by X-ray photoelectron

spectroscopy (XPS) and time of flight – secondary ion mass spectrometry (ToF-SIMS) was used to investigate the bonding mechanisms of the 2-MBT molecule to the copper surface, including the role of the native oxides in the formation of the organic inhibitor layer, the effect of increased exposure time to the inhibitor, and the stability of the organic inhibitor layer upon anodic polarisation.

2. Experimental

Polycrystalline samples obtained from high-purity cast electrolytic tough pitch copper (ETP-Cu) were used [20], [33], [34]. The samples were mechanically polished using silicon carbide papers up to 4000 grit, followed by diamond pastes down to 0.25 µm using an alcohol-based lubricant to obtain a mirror finish surface. They were then ultrasonically cleaned for 5 minutes in successive baths of acetone, ethanol, and Millipore ultra-pure water (resistivity > 18.2 MΩ.cm). Electrochemical polishing was then applied in 60% orthophosphoric acid (H_3PO_4) solution at a constant voltage of 1.4 V versus a copper counter-electrode for 4 minutes to remove the cold-worked layer and the contaminants that may remain after mechanical polishing [35]. Rinsing was performed with a 10% solution of H_3PO_4, followed by ultra-pure water before drying using nitrogen.

The electrochemical experiments were performed using Kel-F (PCTFE) cells containing approximately 350 µl of the electrolyte and equipped with counter and pseudo-reference electrodes made of platinum. The cells were cleaned prior to each experiment using a solution of sulphuric acid (H_2SO_4) and hydrogen peroxide (H_2O_2) in the volume ratio 2:1, then concentrated nitric acid (HNO_3), and finally rinsed several times in boiling ultra-pure water [36]. The Pt pseudo-reference was calibrated before each experiment (+0.75 V vs SHE). The working electrode area was 0.16 cm² delimited by an O-ring. The experiments were performed using a PicoStat bi-potentiostat and the Picoscan software from Agilent Technologies. The electrolytes were a 10 mM HCl aqueous acid solution of pH 2.3 as the reference solution without the inhibitor and a 10 mM HCl + 0.1 mM 2-MBT aqueous solution of pH 2.6 as the solution with inhibitor. HCl was selected as corrosive electrolyte rather than HNO_3 or H_2SO_4 to avoid the interference of N- and S-containing adsorbed species with 2-MBT in the elemental surface analysis. The low concentration of 2-MBT used was due to its low solubility at low pH. All chemicals used were of analytical grade and supplied by Sigma Aldrich.

Cathodic pre-treatment was performed prior to the experiments in order to reduce the air-formed native oxides (Cu_2O). After immersion at the open circuit potential (OCP), the potential was swept cathodically to the onset of hydrogen evolution (down to -0.05 V vs SHE) and then swept back up to the value of +0.10 V vs SHE with a scan rate of 20 mV/s. This was repeated two times. The anodic dissolution tests were performed by sweeping the potential until the anodic apex of +0.37 V vs SHE, followed by reverse sweeping to -0.05 V vs SHE, and then back to the start point at +0.10 V vs SHE with a scan rate of 20 mV/s. To ensure reproducibility, the electrochemical experiments were repeated three times.

Surface analysis was performed after cathodic pre-treatment, i.e., in the as-obtained cathodically reduced metallic state of the interface (reduced state), and after sweeping the potential to the anodic apex, i.e., in the anodically polarized state (anodic state). Once the electrochemical tests were performed, the cell was disconnected and the samples were rinsed with ultra-pure water, dried using nitrogen, and immediately transferred to the UHV chambers for analysis with XPS and ToF-SIMS.

XPS analysis was performed with a Thermo Electron Escalab 250 Xi spectrometer (base pressure < 10^{-10} mbar), using a monochromated Al Kα X-ray source (hv = 1486.6 eV). The binding energy was calibrated by referring to the Fermi level of the sample. A 900 µm diameter X-ray spot size was used, and the take-off angle of the collected photoelectrons was 90°. Survey spectra were recorded with a pass energy of 100 eV at a step size of 1 eV and high-resolution spectra of the C 1s, O 1s, N 1s, S 2p, Cu 2p, Cl 2p core levels and Cu LMM Auger transition were recorded with a pass energy of 20 eV at a step size of 0.1 eV. Decomposition of the spectra was performed with the Thermo Fischer scientific software Avantage using an iterative Shirley-type background subtraction. The CasaXPS software was used to decompose the Cu Auger spectra. The values of the photoionization cross-sections at 1486.6 eV were taken from the Scofield database [37], the transmission function of the analyser was provided by Thermo Fisher, and the inelastic mean free paths were calculated using the TPP-2M formula [38].

ToF-SIMS analysis was performed using a ToF-SIMS 5 spectrometer (IonTof – Munster Germany) operating at a pressure of 5 x 10^{-9} mbar. Data acquisition and post-processing analysis were performed using the SurfaceLab software v6.5. Analysis was done in high current (HC) bunched mode using Bi^+ primary ions of 25 keV energy at a target current of 1.2

pA over an area of 100 x 100 µm². Depth profiles were obtained by interlacing analysis with sputtering using a Cs^+ ion gun of 0.5 keV delivering a 20 nA target current over a 500 x 500 µm² area. The combined use of Bi^+ primary ions and Cs^+ sputtering ions enabled us to analyse both the organic and inorganic surface layers. Both ion beams were at an incidence angle of 45° with respect to the sample surface and were well-aligned to ensure analysis at the centre of the sputtered crater. Negative secondary ions were recorded. Three measurements were recorded from different regions on each sample to ensure reproducibility.

3. Results and Discussion

3.1 Cathodic pre-treatment

The cathodic pre-treatment curves obtained in the absence and presence of 2-MBT in the 10 mM HCl aqueous solution are presented in Figure 1, with the current density obtained in µA/cm² as the potential is swept cathodically and back. The corresponding cathodic charge from each of these curves was calculated by integrating the current density with respect to time and are presented in Table 1 along with the equivalent thickness of reduced oxides, δ. The latter was calculated using the formula:

$$\delta = \frac{q\, V_m}{z\, F} \qquad \textit{Equation 1}$$

where, q is the charge density (in C/cm²), V_m the molar volume of reacting material (23.9 cm³/mol for Cu_2O), z the number of electrons exchanged (2 per Cu_2O molecule), and F the Faraday's constant (96500 C/mol).

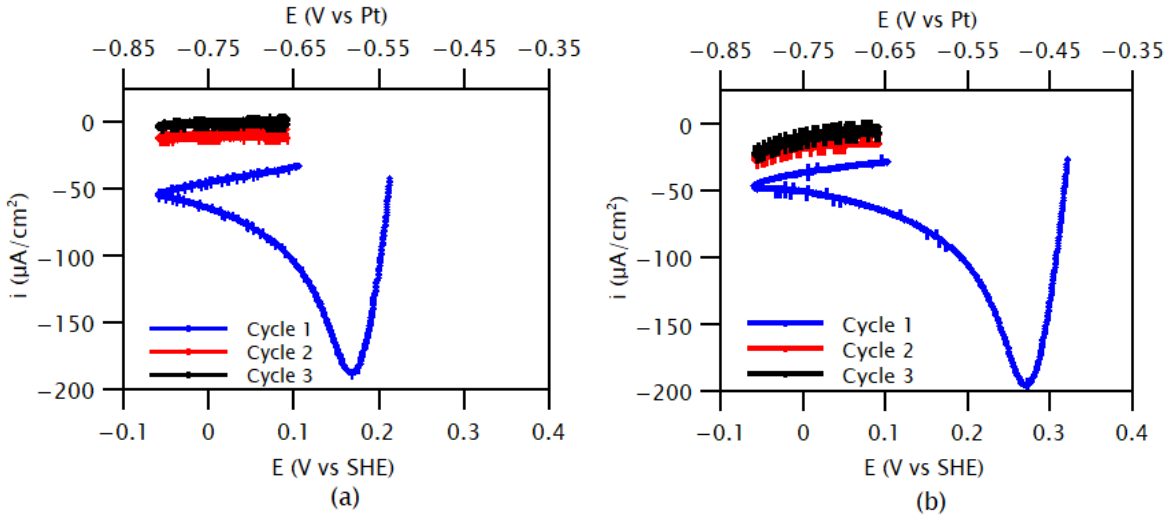

Figure 1: Cyclic voltammograms showing the three cathodic pre-treatment curves of copper obtained with a scan rate of 20 mV/s in (a) 10 mM HCl solution (without inhibitor), and (b) 10 mM HCl + 0.1 mM 2-MBT solution (with inhibitor).

It is observed that for both cases, the first cycle of the cathodic pre-treatment reduces a significant amount of Cu_2O, i.e., more than 2 nm in equivalent thickness. For the pre-treatment in the absence of 2-MBT, the amount of copper oxide reduced in the second cycle is much lower, and nearly negligible in the third cycle reaching an equivalent thickness

markedly less than that of a monolayer of Cu_2O (0.208 nm from the bulk structure). This suggests that all native copper oxide initially present has been reduced, which is supported by the current density value of 0 µA/cm² measured at the end of the third cycle. In these experimental conditions, dissolution of the native oxide is initiated immediately upon immersion in the 10 mM HCl solution, before the first cycle, due to the instability of copper oxide in the low pH of the solution. Therefore, it is likely that the total equivalent thickness of the native oxide is larger than that measured by cathodic pre-treatment. Thus, after the third cycle, a fully metallic state of the copper surface seems achieved in these pre-treatment conditions, although the presence of remaining traces of copper oxide, most likely formed during transfer of the samples in air, is indicated by surface analysis as shown further on.

Table 1: Cathodic charge density (q) and equivalent thickness (δ) of copper oxide reduced during the three cathodic pre-treatment cycles of copper in 10 mM HCl solution (without inhibitor), and in 10 mM HCl + 0.1 mM 2-MBT solution (with inhibitor).

	Pre-treatment in HCl		Pre-treatment in HCl + 2-MBT	
	Charge density q (µC/cm²)	Reduced Cu_2O δ (nm)	Charge density q (µC/cm²)	Reduced Cu_2O δ (nm)
Cycle 1	1697 ± 38	2.10 ± 0.04	1907 ± 78	2.36 ± 0.10
Cycle 2	165 ± 9	0.20 ± 0.01	295 ± 29	0.37 ± 0.04
Cycle 3	32 ± 5	0.04 ± 0.01	185 ± 11	0.23 ± 0.01

The same cannot be said for the cathodic pre-treatment in the presence of the inhibitor. In this case, the total equivalent thickness of Cu_2O reduced in all three cycles is larger, which we assign to less oxide being dissolved upon immersion at OCP in the 2-MBT-containing HCl solution, due to the inhibitive effect 2-MBT molecules adsorbed on the native oxide-covered surface. The third cycle still reduces approximately a monolayer thickness of the native oxides. Additionally, the current density value at the end of the third cycle is slightly negative, which suggests that there were still oxides being reduced at this stage. This lower efficiency of the cathodic pre-treatment in reducing the native oxide within the three cycles is assigned to 2-MBT forming an inhibitor film covering the native oxide surface and poisoning the electrochemical reduction reaction. As a result, oxide islands, protected by the 2-MBT layer, could remain on the metallic substrate. Copper atoms, possibly unreduced, could also be

trapped in the organic layer and form complexes with the 2-MBT molecules, as suggested by previous works reporting the possibility of forming Cu-MBT metal-organic complexes although in different conditions [39], [40].

3.2 Anodic dissolution tests

Figure 2 shows the cyclic voltammograms of anodic dissolution performed for 4 different conditions: (i) in 10 mM HCl without inhibitor, (ii) in 10 mM HCl + 0.1 mM 2-MBT after cathodic pre-treatment in presence of the inhibitor, and (iii) and (iv) also in 10 mM HCl + 0.1 mM 2-MBT but after cathodic pre-treatment in the absence of the inhibitor; (iii) was obtained immediately (2 min) after replacing the 2-MBT-free solution by the 2-MBT-containing solution while (iv) was obtained after 1 hour of exposure to the inhibitor solution.

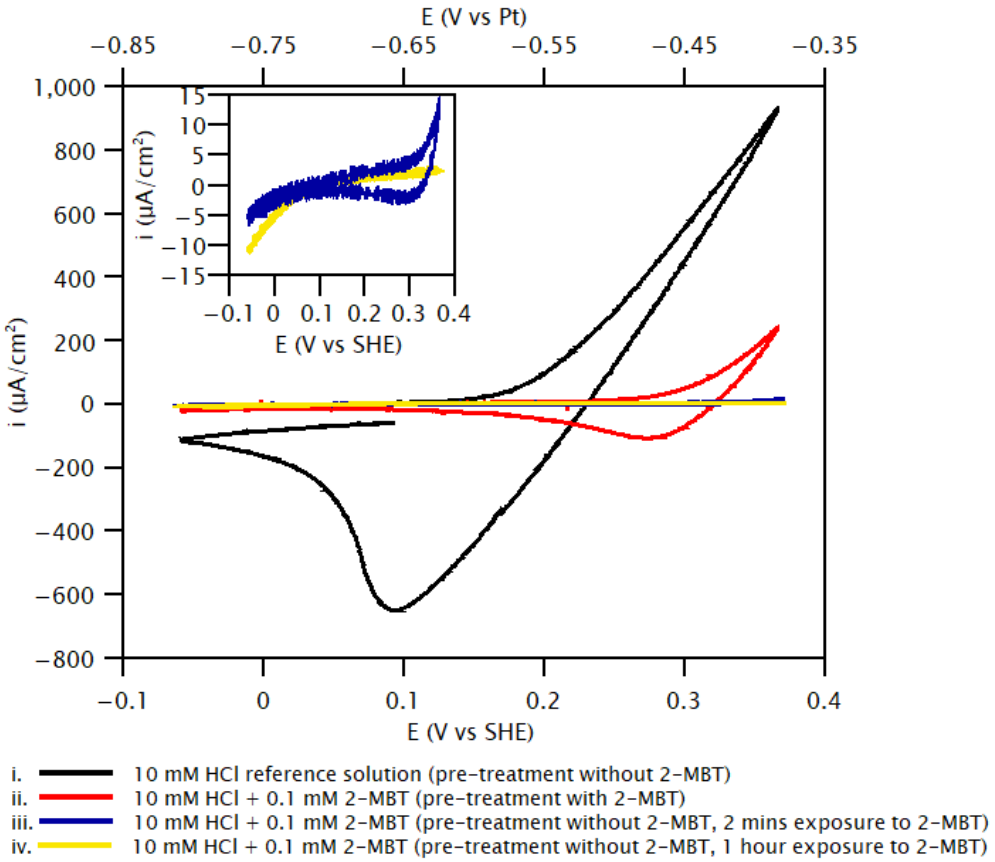

Figure 2: Cyclic voltammograms of copper showing anodic dissolution in the absence or presence of 2-MBT in different pre-treatment conditions (scan rate of 20 mV/s). The inset shows the enlarged cyclic voltammograms of the two experiments performed after pre-treatment without 2-MBT.

For the inhibitor-free reference solution, a very high anodic current density is measured, continuously increasing from approximately +0.15 V vs SHE and indicating the dissolution of copper. $CuCl^-$ or $CuCl_2$ form on the surface of the metal due to the adsorption of chloride ions in these conditions, and the Cu(I) ions dissolve as $CuCl_2^-$, as reported previously [7], [8]. The cathodic sweep exhibits a peak at approximately +0.10V vs SHE, indicating re-deposition of the dissolved copper.

For the CV performed in 10 mM HCl + 0.1 mM 2-MBT after pre-treatment in the presence of 2-MBT, we observe an anodic shift in the initiation of dissolution to about +0.25 V vs SHE, and a lower rise of the anodic current density. This indicates protection of the copper metal surface against anodic dissolution by the organic film of 2-MBT molecules formed at the surface, as previously observed and discussed [20].

Table 2: Anodic and cathodic charge densities determined from the anodic dissolution tests along with the equivalent thickness of copper metal reacting and irreversibly dissolved during the test and calculated from Eq. 1.

Electrolyte, pre-treatment	Anodic charge q_a (µC/cm²)	Cathodic charge q_c (µC/cm²)	Cu reacting (nm)	Cu dissolved (nm)
HCl ref w/o 2-MBT	7032 ± 13	4503 ± 55	5.17 ± 0.01	1.86 ± 0.03
HCl + 2-MBT with 2-MBT	733 ± 24	704 ± 31	0.54 ± 0.02	0.02 ± 0.01
HCl + 2-MBT w/o 2-MBT	52 ± 7	28 ± 2	0.04 ± 0.01	0.02 ± 0.01
HCl + 2-MBT w/o 2-MBT, 1 hr	38 ± 1	28 ± 4	0.03 ± 0.01	0.01 ± 0.01

The CVs performed after pre-treatment in absence of 2-MBT, enlarged in the inset of Figure 2, show even better protection performance for the inhibitor on copper in acidic chloride conditions. The 2 CVs exhibit much flatter curves as well as larger anodic shifts compared both to the reference solution (10 mM HCl) and the CV performed after pre-treatment in presence of inhibitor (10 mM HCl + 0.1 mM 2-MBT). This indicates that the absence of inhibitor during cathodic pre-treatment results in the formation of a less defective and consequently more protective organic barrier layer. The even flatter curve of the CV obtained after 1 hour exposure to 2-MBT before anodic polarization indicates optimization of the barrier properties

with increased exposure time. Complementary measurements (**Erreur ! Source du renvoi introuvable.** in Supplementary Information) show that the barrier properties are already optimized after 15 minutes of exposure to 2-MBT after cathodic pre-treatment in the inhibitor-free solution.

The anodic and cathodic charges for each curve were calculated by integrating the anodic and cathodic current densities, respectively, with respect to time, and the equivalent thicknesses of Cu metal reacting and dissolved during the cycle were determined using Equation 1. Results are compiled in Table 2. The amount (equivalent thickness) of Cu dissolved was deduced from the difference between anodic and cathodic charge densities ($q_a - q_c$). For each experiment with 2-MBT, the anodic charge and therefore the equivalent thickness of reacting copper decrease markedly, by a factor of 10 between the test in reference solution and the test performed after pre-treatment with inhibitor, by another factor of 14 after pre-treatment without inhibitor, and finally by an additional factor of 1.4 after pre-treatment without inhibitor followed by 1 hour exposure to the inhibitor. This evidences that controlling the conditions of formation of the inhibiting barrier layer by electrochemical means and minimizing the presence of native oxides does play an important role in the mitigation of the dissolution of copper and is instrumental for optimizing the barrier properties of the interfacial organic film.

ToF-SIMS depth profiling of the inhibiting interface

Surface analysis by ToF-SIMS and XPS was applied to the inhibiting interfaces formed in the 2-MBT-free HCl reference solution and those formed in the 2-MBT-containing HCl solution after cathodic pre-treatment in presence or absence of the inhibitor. In the latter case of pre-treatment in absence of 2-MBT, the interface was optimized by 1 hour exposure to 2-MBT after performing the cathodic pre-treatment in the inhibitor-free solution. Hereafter, we discuss the ToF-SIMS depth profiling data shown in Figure 3 for the inhibiting interfaces obtained in the cathodically reduced metallic state. Those obtained after anodic polarization are shown in Supplementary Information (**Erreur ! Source du renvoi introuvable.**). The differences, quantified by XPS analysis, are discussed in the next section.

The ToF-SIMS depth profiles in Figure 3 display the intensity of the selected secondary ions plotted in logarithmic scale vs the sputtering time, the latter being related to the depth from

the initial topmost surface. The selected ions were $C_7H_4NS_2^-$, C_2N^-, C_2S^-, and $^{34}S^-$ ions, characteristic of the 2-MBT molecule, its fragments of nitrogen, its fragments of sulphur, and the overall sulphur, respectively. Additionally, Cu^-, O^-, Cu_2O^-, $^{37}Cl^-$ ions were selected as they are characteristic of the metallic substrate, the oxides, and the chlorine adsorbed on the surface. The positions of each interface or layer was defined by the maximum intensity of the corresponding ions with an uncertainty of 5%.

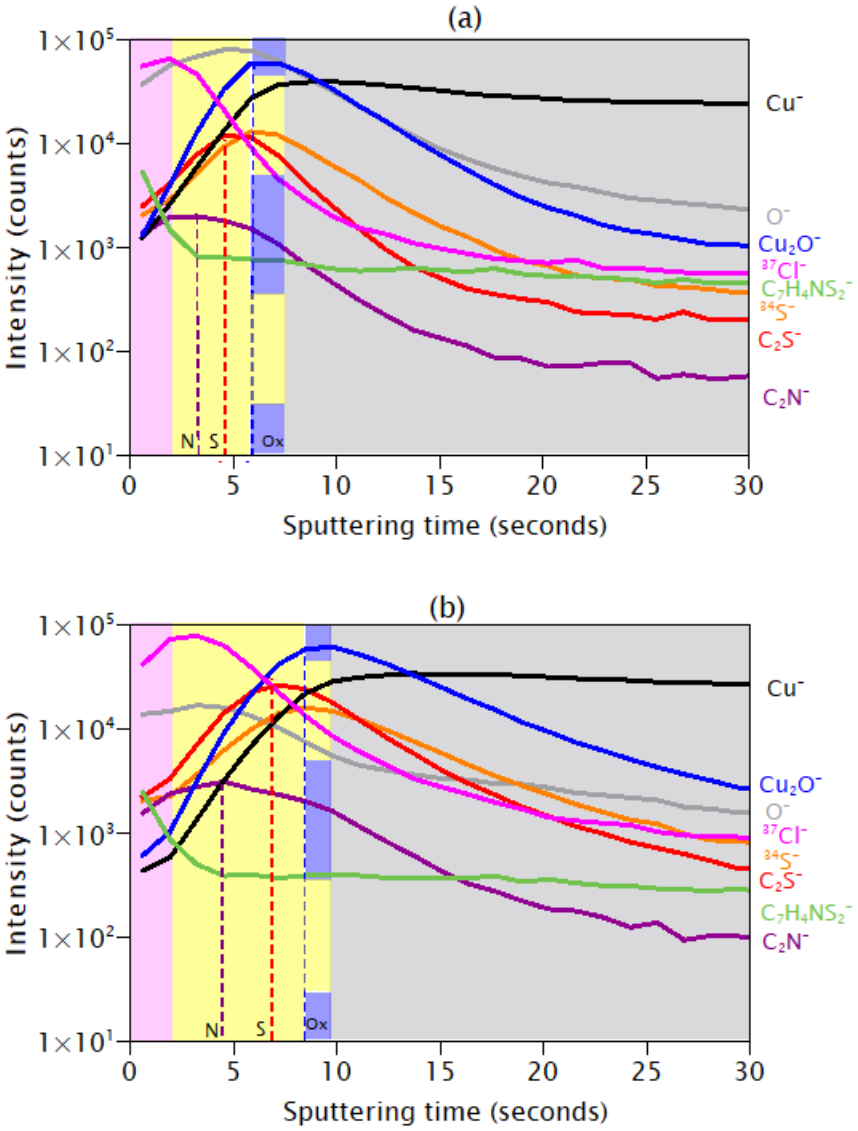

Figure 3: ToF-SIMS depth profiles of the inhibiting interface obtained in reduced state (a) after cathodic pre-treatment with 2-MBT, and in reduced state (b) after cathodic pre-treatment without 2-MBT followed by 1 hour of exposure to the inhibitor.

Cu^- being more characteristic of metallic Cu, was used to define the position where the metallic Cu substrate is reached. It corresponds to 7 and 10 seconds of sputtering time after

pre-treatment with and without 2-MBT, respectively. On both depth profiles, the organic layer, characterized by the $C_7H_4NS_2^-$, C_2N^- and C_2S^- ions, covers the metallic substrate, which confirms that 2-MBT is adsorbed on the metallic substrate. However, it can be noticed that the intensity of the $C_7H_4NS_2^-$ ions is maximum at the topmost surface, whereas those of the C_2N^- and C_2S^- ions are maximum in the inner part of the organic layer. This indicates, that 2-MBT forms multilayers with an inner chemisorbed layer (yellow regions on the profiles) and an outer physisorbed multilayer (pink regions on the profiles), as observed previously for adsorption of the molecule from the gas phase [22], [24], [26], [32] and in neutral aqueous solution [28]. The position of the C_2S^- intensity maximum is closer to the substrate than that of the C_2N^- intensity maximum, which indicates that 2-MBT bonds to the surface via the two S atoms, in agreement with the work of Vernack et al. [28].

Interestingly, the Cu_2O^- signal exhibits a maximum intensity slightly before reaching the metallic Cu region (Cu^-). This indicates that, although the reduction pre-treatment was applied, Cu oxide islands (marked in blue on the profiles) remain locally on the surface, in agreement with the electrochemical analysis above. The $^{34}S^-$ secondary ions, characteristic of sulphur atoms from the intact and/or dissociated molecules, peak at a larger depth than the C_2S^- ions, characteristic of the intact molecule, and concomitantly with the CuO_2^- ions, indicating that sulphur atoms are also bonded to the metal surface. Since the C_2S^- ions curve remains behind the C_2N^- curve, there is no indication of the nitrogen atoms bonding to copper.

Looking at the Cl^- signal, one observes that it exhibits its maximum intensity in the outer region (marked in pink), assigned to the physisorbed MBT layer. However, the intensity of Cl^- signal decreases strongly in the inner chemisorbed MBT layer (marked in yellow). This is consistent with the chemisorbed MBT layer drastically reducing the interaction of chlorine with the copper substrate by acting as a physical barrier between them.

The differences in the depth profiles of both experiments relate to the thickness of the interface. A thicker 2-MBT organic layer is observed in the case of pre-treatment without 2-MBT followed by 1 hour exposure to the inhibitor (Figure 3(b)) than in the case of pre-treatment with 2-MBT (Figure 3(a)), which would enhance the efficiency of the protection against dissolution as revealed by the anodic polarization tests.

3.4 XPS analysis of interfacial bonding and thickness

Figure 4 shows the XPS Cu 2p, Cl 2p, S 2p, C 1s, N 1s and O 1s core level spectra obtained in this work, in this case after exposure to the solution of 10 mM HCl + 0.1 mM 2-MBT in reduced state, after pre-treatment in the presence of 2-MBT. A summary of the elemental components observed in this work with their binding energies (BE), full widths at half maximum (FWHM), and assignments is given in Table 3. The assignment of the components from the 2-MBT molecule are depicted in Figure 5.

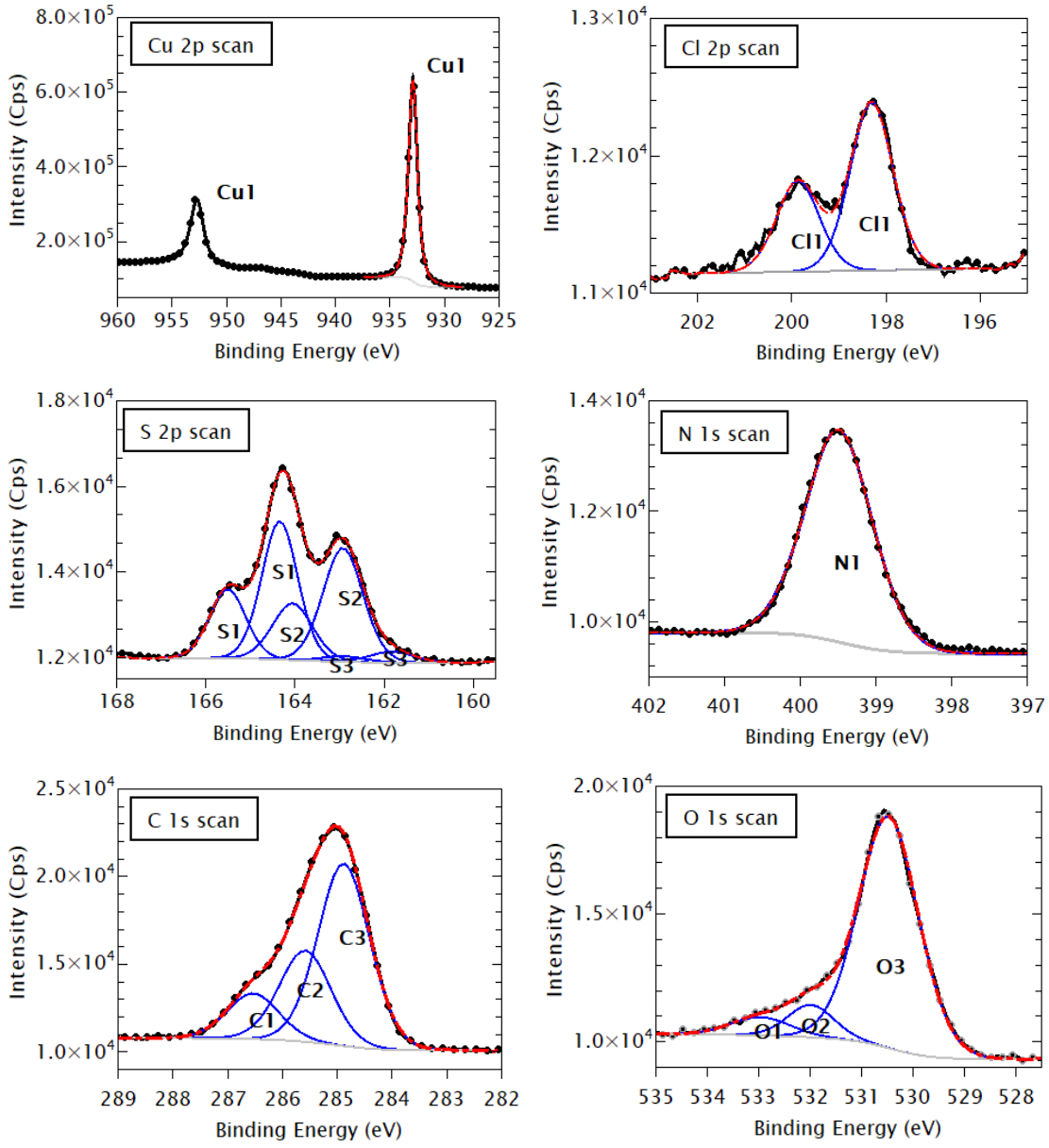

Figure 4: XPS Cu 2p, Cl 2p, S 2p, N 1s, C1s, and O 1s core level spectra after exposure to the solution of 10 mM HCl + 0.1 mM 2-MBT in reduced state, after pre-treatment in the presence of 2-MBT.

The copper Cu 2p spectrum showed the $2p_{3/2}$ - $2p_{1/2}$ spin-orbit doublet at 932.8 - 952.6 eV BE. The $2p_{3/2}$ component can correspond to three states that are too close to be resolved: the Cu(0) metallic state at 932.6 eV, the Cu(I) oxidized state at 932.7 eV, and Cu_2S at 932.9 eV [41], [42]. Cu(II) oxide is not observed in this spectrum; it would appear at 933.5 eV along with satellite peaks, which are characteristic of the Cu(II) oxide [41], [42]. Analysis of the Cu composition using the Cu LMM Auger spectrum is discussed below.

Table 3: Elemental core levels and Auger transition components observed in XPS analysis from this work with their Binding Energies (BE) / Kinetic Energies (KE), Full Width at Half Maximum (FWHM) and their assigned chemical states. Uncertainty ranges are derived from the uncertainty of the curve fitting procedure.

Peak component		BE (± 0.1 eV)	FWHM (± 0.2 eV)	Assignment
Cu $2p_{3/2}$		932.8	1.0	Cu $2p_{3/2}$
		932.6		Cu(0) metal [41], [42]
		932.7		Cu(I) oxide [41], [42]
		932.9		Cu(I) sulphide [41], [42]
N 1s		399.4	1.1	N not bonded to metallic Cu
S $2p_{3/2}$	S1	164.2	1.0	Endocyclic S not bonded to metallic Cu (2-MBT)
	S2	162.8	1.0	Exocyclic S not bonded to metallic Cu (2-MBT)
	S3	161.9	1.0	S bonded to metallic Cu
C 1s	C1	286.4	1.1	C=S, residual contamination
	C2	285.5	1.1	C-N, C-S
	C3	284.8	1.1	C-C, C-H
O 1s	O1	532.9	1.6	H_2O adsorbed
	O2	531.4	1.4	OH
	O3	530.2	1.4	O from metal oxide (Cu_2O)
Cl $2p_{3/2}$	Cl1	198.3	1.1	Adsorbed chlorine
	Cl2	199.0	0.9	Copper chloride (CuCl)
Cu LMM	Cu (0)	918.4 (KE)		Cu metal
	Cu (I)	916.6 (KE)		Cu oxide

The Cl 2p spectrum was decomposed in $2p_{1/2}$ - $2p_{3/2}$ spin-orbit doublets with a branching ratio of 0.5 and splitting of 1.60 eV. The Cl $2p_{3/2}$ (Cl1) component at 198.3 eV corresponds to chlorine adsorbed on the surface [43], [44]. Another Cl $2p_{3/2}$ component (Cl2), at a binding

energy of 199.0 eV and corresponding to CuCl [44], was only observed after anodic polarization in the 2-MBT-free HCl reference solution, as shown in **Erreur ! Source du renvoi introuvable.** given in Supplementary Information. This is consistent with the inhibition properties of 2-MBT blocking the access of chloride ions to the copper substrate surface and thus preventing the formation of CuCl surface species.

$2p_{1/2}$ - $2p_{3/2}$ spin-orbit doublets, with a branching ratio of 0.5 and splitting of 1.18 eV, were also considered for peak fitting the S 2p spectrum. Three components/chemical states, labelled S1, S2, and S3, were observed in agreement with previous work [24]. The S1 component at 164.2 eV corresponds to the endocyclic sulphur from the 2-MBT molecule not bonded to metallic copper. The S2 component at 162.8 eV corresponds to the exocyclic sulphur from the molecule, also not bonded to metallic copper. These two components can also correspond to the S atoms of the molecules bonded to copper oxides and/or forming multilayers physically adsorbed on the surface [13], [24], [28], [32]. The S3 component at 161.9 eV is sulphur bonded directly to metallic copper, which was also observed when exposing a clean metallic Cu surface to H_2S [41]. This component can originate from either of the two sulphur atoms, endocyclic or exocyclic, from the intact molecules bonded to metallic copper. It can also be free sulphur atoms that have dissociated from the molecule and then bonded to metallic Cu [22], [24], [32].

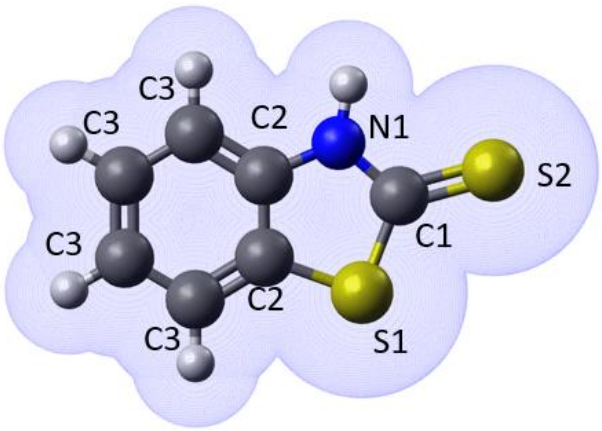

Figure 5: 2-MBT chemical structure (thione form) and the assigned chemical states of the components obtained from their respective binding energies during XPS analysis.

The N 1s spectrum was fitted with one peak component observed at 399.4 eV and originating from the nitrogen atoms of the molecules that are not bonded to copper [13], [24]. From

previous work, we know that the N bonded to Cu is expected at 399.8 eV [24]. The slight shift observed in the BE (+0.3 eV) compared to other in situ XPS studies is most likely due to the influence of the exposure to air during transfer to XPS [22], [25].

The carbon C 1s spectrum was decomposed into three peaks/chemical states. The C1 component at 286.4 eV corresponds to C=S bonds in the molecule, the C2 component at 285.5 eV to C-N and C-S bonds, and the C3 component at 284.8 eV to C-C and C-H bonds in the benzene ring [13], [24]. Since the carbon atoms in these chemical states are in the ratio 1:2:4 in the 2-MBT molecule, the experimental observation of this intensity ratio is indicative of the adsorption of most of the 2-MBT molecules in the intact form, like in previous experiments of adsorption from the gas phase [24].

Table 4: Normalized intensities (NI) (±3%) and relative intensities (RI) of the elemental core level components and Auger transition highlighting the changes between the two pre-treatment methods and their respective reduced and anodic states.

Peak component		Pre-treatment with 2-MBT				Pre-treatment without 2-MBT			
		Reduced state		Anodic state		Reduced state		Anodic state	
		NI (a.u.)	RI (%)	NI (a.u.)	RI (%)	NI (a.u.)	RI (%)	NI (a.u.)	RI (%)
N 1s		0.27	100	0.26	100	0.44	100	0.39	100
S $2p_{3/2}$	S1	0.31	50	0.30	49	0.50	49	0.46	48
	S2	0.29	45	0.27	45	0.46	45	0.39	41
	S3	0.03	5	0.04	6	0.06	6	0.11	11
C 1s	C1	0.34	14	0.44	14	0.51	14	0.48	14
	C2	0.68	29	0.88	29	1.03	29	0.96	29
	C3	1.35	57	1.76	57	2.06	57	1.92	57
O 1s	O1	0.04	5	0.14	15	0.15	44	0.08	13
	O2	0.13	15	0.32	33	0.07	20	0.21	35
	O3	0.70	80	0.50	52	0.12	36	0.32	52
Cu LMM	Cu(0)	12.39	84	12.20	89	10.27	95	10.56	89
	Cu(I)	1.93	16	1.19	11	0.40	5	1.09	11

The oxygen O 1s spectrum was decomposed into three components: O1 at 532.9 eV corresponding to oxygen adsorbed on the surface from water and/or from exposure to air, O2 at 531.4 eV from hydroxides formed on the surface, and O3 at 530.2 eV from the oxygen atoms of the copper oxide matrix, Cu_2O in this case [22], [32], [41], [42]. From the XPS survey spectra (not shown), it was also determined that there was essentially no presence of residual phosphorous from the electrochemical polishing process indicating no interference of this procedure on the experiments.

Table 4 compiles the normalized intensities (±3%) and the relative intensities of the elemental components according to the electrochemical conditions of formation and treatment of the interface. It is observed that the relative intensities of the C 1s components always remain in the molecular ratio mentioned above. The N 1s component also remains unchanged owing to the presence of only one chemical state, i.e. N not bonded to Cu. However, we do observe a change in the relative intensities of the O 1s, Cu LMM, and S 2p components. The O3 component assigned to metal oxide (Cu_2O) has a similar trend to the Cu(I) component from the Cu LMM spectrum discussed next. The changes observed in the relative intensities of the S 2p components are discussed subsequently.

Since the Cu(I) oxide component is indistinguishable from the Cu(0) metal component in the Cu 2p spectrum, we also recorded and decomposed the Cu LMM Auger spectrum in order to discriminate the contributions of copper oxide and copper metal. The Cu LMM Auger spectrum obtained in different interfacial conditions are shown in Figure 6. They were decomposed by peak fitting using the line-shapes of Cu(0) and Cu(I) obtained from reference spectra measured on metallic Cu and oxidized samples in the same analytical conditions, as done by others [32], [41], [45].

We can observe in Figure 6(a) that, although the intensity of Cu(I) is quite weak compared to that of Cu(0) , it is markedly higher than that in Figure 6(c) where the cathodic pre-treatment was done in absence of the inhibitor. This agrees with the electrochemical analysis from which we deduced more efficient reduction of the native oxides by cathodic pre-treatment in absence of the inhibitor. In Figure 6(b), we observe a decrease in the Cu(I) intensity after anodic polarization (anodic state) compared to that measured after cathodic pre-treatment (reduced state) in Figure 6(a). This is indicative of dissolution of the oxide remnants during polarization followed by additional adsorption of 2-MBT molecules, as observed by the slight

increase in relative intensity of the S3 component (S bonded to metallic Cu) in Table 4. In Figure 6(c), the almost negligible Cu(I) intensity is consistent with the lower intensity O3 component in the O 1s spectrum (Table 4). It cannot be fully excluded that these oxide traces result from re-oxidation of the surface during air transfer due to the imperfections in the organic barrier film formed by 2-MBT after electrochemical preparation. After anodic polarization (Figure 6(d)), we observe an increase in the Cu(I) intensity. It is proposed that during polarization, defects are formed on the organic barrier layer. These unprotected regions would re-oxidize during air transfer after the experiment.

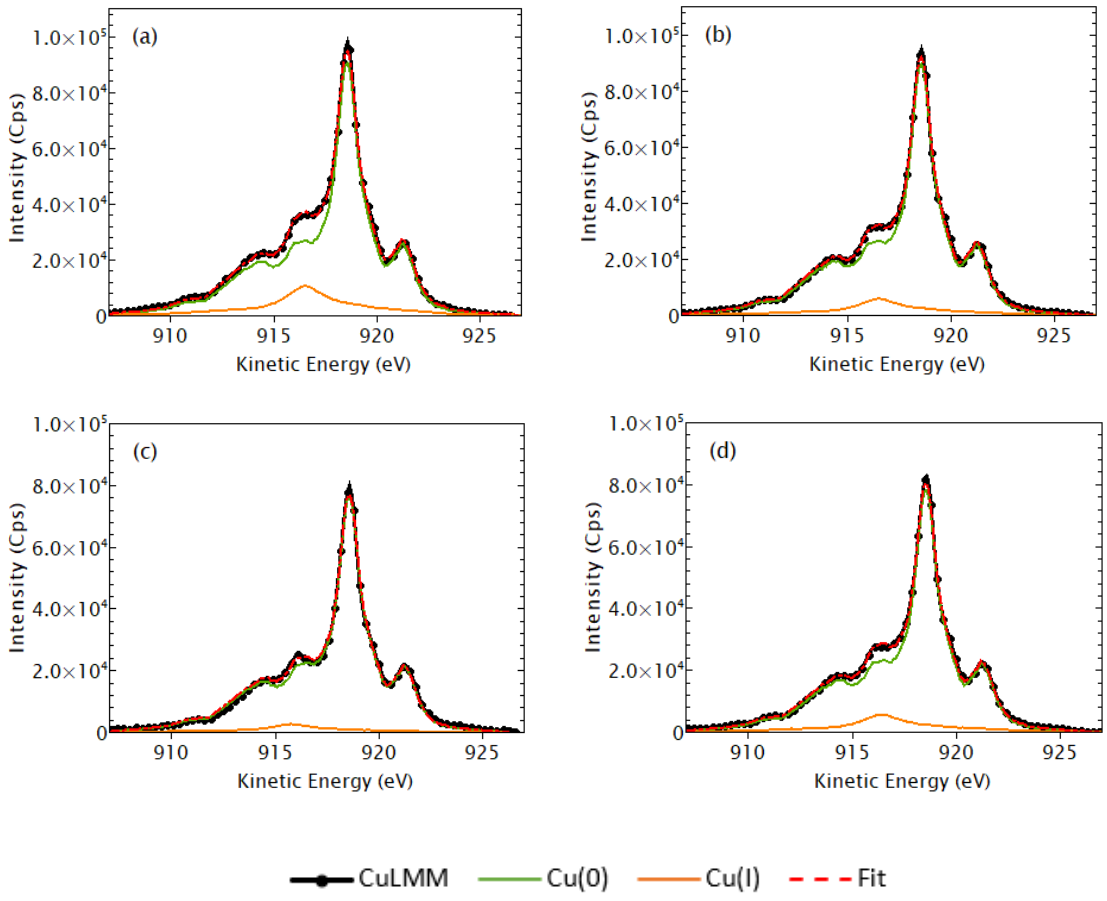

Figure 6: Cu LMM Auger spectra obtained for experiments done in 10 mM HCl + 0.1 mM 2-MBT at (a) reduced state, pre-treatment with MBT, (b) anodic state, pre-treatment with MBT, (c) reduced state, pre-treatment w/o MBT, 1 h MBT exposure, (d) anodic state, pre-treatment w/o MBT, 1 h MBT exposure.

Using the intensities of the Cu 2p, O 1s, N 1s, S 2p spectra, we performed quantitative analysis applying a bi-layer model of attenuation of the photoelectron intensity in order to estimate the thickness of the organic inhibitor layer and the coverage and thickness of the residual oxide islands present at the interface. A schematic of the bi-layer model used is shown in

Figure 7. This model, taking oxide islands into consideration, as deduced from the ToF-SIMS and XPS measurements indicating the presence of islands of oxides and sulphur bonding to metallic Cu, allows us to further discuss the effects of the electrochemically controlled conditions of formation of the interface on its inhibition properties.

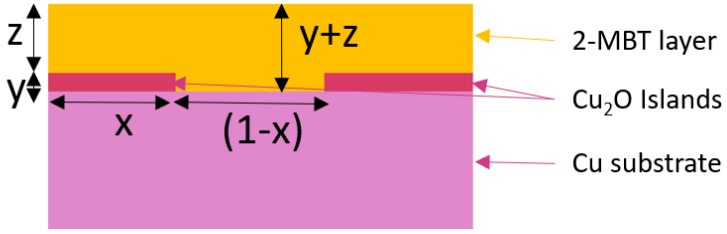

Figure 7: Schematic showing the model used to determine the thickness and coverage of the oxide islands, the thickness of the 2-MBT layer above the oxide islands and above the metallic copper.

The oxide islands, above the copper substrate of infinite thickness ("infinite" meaning much thicker than the escape depth of the analysed photoelectrons), were assumed to have uniform thickness. The 2-MBT organic layer covers both the oxide islands and the metallic copper surface in-between, as indicated by the Tof-SIMS depth profiles. The 2-MBT organic layer surface has the same flatness as the substrate surface. From this model, we can extract the coverage (x) and thickness (y) of the oxide islands, and the thickness of the 2-MBT layer above the oxide islands (z) and above the metallic copper (y+z). The equations used in this modelling method are given in Supplementary Information. Although this model results in high uncertainties for the extracted values, the results are comparable between the experiments, and in conjunction with the intensities (normalized and relative intensities) of the components reported in Table 4. For the sake of easier comparison, the equivalent thickness of the oxide and 2-MBT layers were calculated by weighting the thickness with the coverage of each layer. Table 5 compiles the obtained values. A graphical display of the results is presented schematically in Figure 8.

It is observed that whatever the pre-treatment conditions, with 2-MBT or without 2-MBT (and subsequent 1 hour exposure to 2-MBT), the coverage of oxide islands is high, and their thickness relatively low (less than 0.5 nm), the latter even reaching 0.14 nm in the reduced state of the interface after pre-treatment without 2-MBT which is less than a monolayer (0.208 nm). In these optimized conditions of formation of the interface (Figure 8 c-d), the equivalent thickness of the remaining oxide is 0.11 nm, also lower than that of a monolayer,

suggesting that the actual coverage of remaining oxide islands is overestimated with our model, possibly due to inhomogeneous thickness of the oxide islands. This significant decrease in the amount of oxide remaining at the interface agrees with the electrochemical data presented above and with the variation of the Cu LMM Auger line-shape measured by XPS in Figure 6 c-d. It supports our explanation that, when present during pre-treatment, the 2-MBT molecules, pre-adsorbed on the oxide surface, poison the electrochemical reduction reaction which results in significantly more oxide trapped at the interface.

Table 5 : Coverage and thickness values of the copper oxide islands and 2-MBT organic inhibitor layer determined from quantitative analysis of the XPS results using the bi-layer model. The uncertainty on the coverage was estimated to be ± 10%, and the uncertainty on the thicknesses were estimated to be ± 0.2 nm.

Exp. no.	Electrochemical conditions	Coverage of Cu_2O islands (%)	Thickness of Cu_2O islands (nm)	Equivalent thickness of Cu_2O (nm)	Thickness of 2-MBT layer above oxides (nm)	Thickness of 2-MBT layer above metallic Cu (nm)	Equivalent thickness of 2-MBT layer (nm)
1	Pre-treatment with MBT, reduced state	90	0.47	0.42	0.97	1.44	1.02
2	Pre-treatment with MBT, anodic state	87	0.36	0.31	0.98	1.34	1.03
3	Pre-treatment w/o MBT, 1 h MBT exposure, reduced state	78	0.14	0.11	2.19	2.33	2.22
4	Pre-treatment w/o MBT, 1h MBT exposure, anodic state	62	0.38	0.24	1.94	2.32	2.08

The oxide traces observed after pre-treatment without 2-MBT in the solution could result from incomplete efficiency of the applied conditions despite the absence of remaining oxide indicated by the electrochemical data. As stated above, re-oxidation of the 2MBT-protected surface during air-transfer for surface analysis cannot be fully excluded. Additionally, Table 5 (Figure 8) also shows that the 2-MBT layer is significantly thicker in the case of pre-treatment without the inhibitor with subsequent 1 hour exposure to 2-MBT. This indicates that lower quantities, including lower coverage, of remaining interfacial oxide on the surface, possibly along with the increased exposure time to the inhibitor molecule, enhance the deposition of

multilayers of the organic molecule on the surface, resulting in thicker and better protective barrier layers.

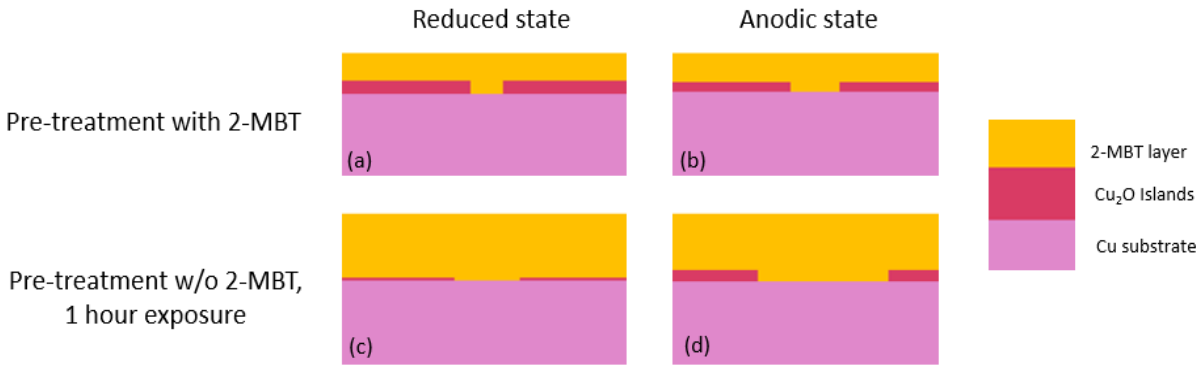

Figure 8: Schematic showing the differences in coverage and thickness of the oxide islands and thickness of the 2-MBT layer as determined from XPS surface analysis for (a) reduced state, pre-treatment with MBT, (b) anodic state, pre-treatment with MBT, (c) reduced state, pre-treatment w/o MBT, 1 h MBT exposure, (d) anodic state, pre-treatment w/o MBT, 1 h MBT exposure.

After anodic polarization of the interface with more remaining oxide, i.e., cathodically pre-treated with 2-MBT (Figure 8 a-b), it is observed that the oxide islands thickness slightly decreases whereas their coverage remains nearly unchanged. It is proposed that, due to the formation of defects in the 2-MBT barrier layer upon anodic polarization, the acidic electrolyte (pH = 2.6) may penetrate the barrier layer, access the oxide surface, and thus at least partially dissolve the interfacial oxide layer. This alteration of the barrier properties of the 2-MBT layer is reflected by a slight decrease in thickness of the interfacial oxide (Table 5). In the experiment where the interface is cathodically pre-treated in the absence of 2-MBT (Figure 8 c-d), the quantities of the remaining oxides are extremely low to begin with. After anodic polarization, defects are formed in the 2-MBT layer but there is little to no oxide beneath to dissolve. Once the sample is removed from the cell and transferred in air for analysis, the defective areas formed in the 2-MBT barrier layer do not protect the surface from re-oxidation, and thus thicker islands of oxides are locally formed (Table 5, Figure 8).

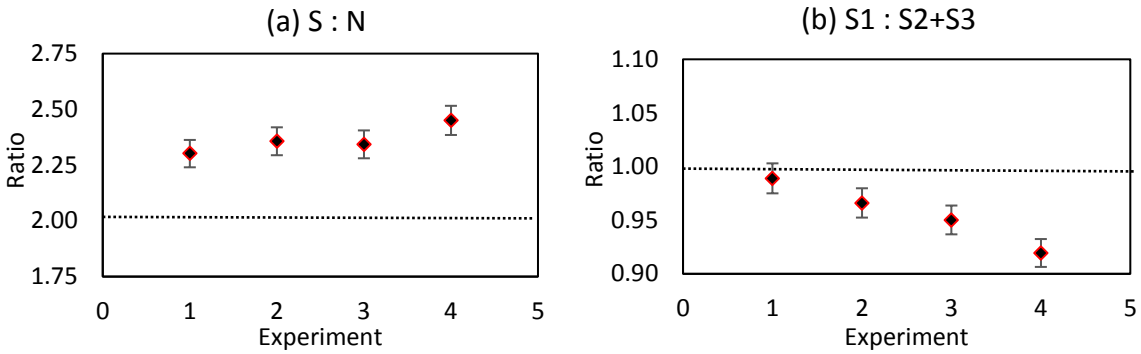

Figure 9: Atomic ratios of (a) S : N, and (b) S1 : S2+S3, determined from the component intensities of the XPS S 2p and N 1s spectra. (Exp. 1) Pre-treatment with MBT, reduced state, (Exp. 2) Pre-treatment with MBT, anodic state, (Exp. 3) Pre-treatment w/o MBT, 1 h MBT exposure, reduced state, (Exp. 4) Pre-treatment w/o MBT, 1 h MBT exposure, anodic state.

In previous work on 2-MBT deposited from the gas phase, it has been shown that sulphur could dissociate from the molecule and bond with metallic copper in the form of free atomic sulphur detected as part of the S3 component in the XPS S 2p core level spectrum [24]. In order to determine if this is also the case in the present experiments, atomic ratios between sulphur and nitrogen were calculated. In the 2-MBT molecule, the stoichiometric ratio between these elements is 2:1. However, from quantitative analysis of the XPS data, we determine that we always have an excess of sulphur, as shown in Figure 9, confirming that, in our case, we also have free sulphur atoms that are bonded to the metal. Therefore, the S3 component in the S 2p spectrum corresponds to both the molecule bonded to metallic copper via its S atoms as well as to free sulphur atoms bonded to the metallic copper surface. We also observe in Figure 9(a) that there is a trend to an increase in sulphur in the anodic state compared to the cathodically reduced state in either case of pre-treatment. Hence, it is suggested that during anodic polarization some of the 2-MBT molecules tend to dissociate resulting in free sulphur atoms bonded to the metallic copper surface. This alteration appears consistent with formation defects of the protective 2-MBT layer, compromising its barrier properties.

The origin of the S3 component was determined by analysing the atomic ratio between the S1, S2 and S3 components (Figure 9(b)). It was determined that the ratio between S1 and the combination of S2 and S3 components result in a value close to 1, which is the proper ratio between the endocyclic S1 and exocyclic S2 sulphur. Therefore, it is suggested that the S3 component mainly comes from S2, the exocyclic sulphur from the 2-MBT molecule. We

observe in Figure 9(b) that after anodic polarization in either pre-treatment condition of the interface, there is a slight decrease in this ratio, indicating that the quantity of S1 has decreased. This suggests that during anodic polarization, this is the endocyclic sulphur (S1 component) in some of the 2-MBT molecules that tends to dissociate to give free sulphur bonded to metallic copper (along with dissociated S2 exocyclic sulphur) in the defective regions of the barrier layer. This is also observed in Table 4 by the relative intensities of the sulphur components where we also observe a decrease in the S1 and S2 components but an increase in the S3 component after anodic polarisation for both the experiments. This results in an increased coverage in the bonding between the 2-MBT molecule/sulphur atoms and the metallic copper substrate after anodic polarisation, as seen in Table 5, Figure 8.

4. Conclusions

The formation of the 2-MBT inhibiting interface by electrochemical cathodic control and how it enhances the corrosion resistance of copper in an acidic environment was investigated by applying electrochemistry and advanced surface analysis. The barrier properties of the 2-MBT organic protective layer are highly influenced by the cathodic pre-treatment protocol applied to reduce the native oxide initially present on the copper surface. Advanced elimination of the native oxide, as confirmed by ToF-SIMS and XPS, promotes the formation of a thicker, and likely less defective, inhibitor multilayer, more protective in the anodic dissolution regime of copper. Enhanced inhibition is obtained when the cathodic pre-treatment is performed in the inhibitor-free solution prior to time optimization of 2-MBT adsorption under cathodic control of the interface. When performed in an inhibitor-containing solution, the cathodic pre-treatment is less effective in fully reducing the native oxide, owing to mitigation of the reduction reaction by pre-adsorption of 2-MBT on the oxidized surface.

In an acidic environment, the 2-MBT molecules (thione conformer) bond to both metallic copper and residual copper oxide islands via their sulphur atoms. No signature of bonding via the nitrogen atom was found from XPS, in agreement with ToF-SIMS. An excess of sulphur was observed from XPS (S3 component from S 2p spectrum), indicating partial dissociation of the molecules to release atomic sulphur, mostly originating from the exocyclic S atoms and

bonded to metallic copper exposed in between the residual oxide islands. Upon anodic polarisation, a trend of further dissociation of the inhibitor molecule was observed, which was reflected by increased coverage of sulphur bonded to metallic copper, now mostly originating from the endocyclic S atoms. This anodic alteration of the protective 2-MBT layer would induce the formation of defects, thus compromising the barrier properties, as suggested by the ex-situ in-air reactivity of the interface.

Credit authorship contribution statement

Vishant Garg: Investigation, Formal analysis, Writing – original draft, review & editing.

Sagar Sharma: Preliminary Investigation

Sandrine Zanna: Investigation, Validation, Writing – review & editing.

Antoine Seyeux: Investigation, Validation, Writing – review & editing.

Frédéric Wiame: Conceptualization, Validation, Writing – review & editing, Supervision.

Vincent Maurice: Conceptualization, Validation, Writing – review & editing, Supervision, Funding acquisition.

Philippe Marcus: Conceptualization, Writing – review & editing, Supervision, Funding acquisition, Project management.

Declaration of Interest

The authors declare that they have no known competing financial interests or personal relationships that could have appeared to influence the work reported in this paper.

Acknowledgements

This project has received funding from the European Research Council (ERC) under the European Union's Horizon 2020 research and innovation program (ERC Advanced grant no. 741123).

References

[1] H.-H. Strehblow and A. Titze, “The investigation of the passive behaviour of copper in weakly acid and alkaline solutions and the examination of the passive film by ESCA and ISS,” *Electrochim Acta*, vol. 25, no. 6, pp. 839–850, 1980.

[2] J. Kunze, V. Maurice, L. H. Klein, H. H. Strehblow, and P. Marcus, “In situ scanning tunneling microscopy study of the anodic oxidation of Cu(111) in 0.1 M NaOH,” *Journal of Physical Chemistry B*, vol. 105, no. 19, pp. 4263–4269, May 2001, doi: 10.1021/jp004012i.

[3] V. Maurice and P. Marcus, “Current developments of nanoscale insight into corrosion protection by passive oxide films,” *Curr Opin Solid State Mater Sci*, vol. 22, no. 4, pp. 156–167, Aug. 2018, doi: 10.1016/j.cossms.2018.05.004.

[4] N. Takeno, “Atlas of Eh-pH diagrams Intercomparison of thermodynamic databases,” *Geological survey of Japan open file report*, vol. 419, p. 102, 2005.

[5] S. B. Sharma, V. Maurice, L. H. Klein, and P. Marcus, “In situ scanning tunneling microscopy study of 2-mercaptobenzimidazole local inhibition effects on copper corrosion at grain boundary surface terminations,” *Electrochim Acta*, vol. 378, May 2021, doi: 10.1016/j.electacta.2021.138150.

[6] G. Kear, B. D. Barker, and F. C. Walsh, “Electrochemical corrosion of unalloyed copper in chloride media--a critical review,” *Corros Sci*, vol. 46, no. 1, pp. 109–135, 2004, doi: 10.1016/S0010-938X(02)00257-3.

[7] F. K. Crundwell, “The Anodic dissolution of copper in hydrochloric acid solutions,” *Electrochim Acta*, vol. 31, no. 15, pp. 2701–2714, 1992.

[8] J.-P. Diard, J.-M. le Canut, B. le Gorrec, and C. Montella, “Copper electrodissolution in 1 M HCl at low current densities. I. General steady-state study,” *Electrochim Acta*, vol. 43, no. 16–17, pp. 2469–2483, 1998.

[9] J.-P. Diard, J.-M. le Canut, B. le Gorrec, and C. Montella, “Copper electrodissolution in 1 M HCl at low current densities. II. Electrochemical impedance spectroscopy study,” *Electrochim Acta*, vol. 43, no. 16–17, pp. 2485–2501, 1998.

[10] M. Finšgar, “2-Mercaptobenzimidazole as a copper corrosion inhibitor: Part I. Long-term immersion, 3D-profilometry, and electrochemistry,” *Corros Sci*, vol. 72, pp. 82–89, Jul. 2013, doi: 10.1016/j.corsci.2013.03.011.

[11] A. Shaban, E. Kálmán, J. Telegdi, G. Pálinkás, and G. Dóra, “Corrosion and inhibition of copper in different electrolyte solutions,” *Appl. Phys. A*, vol. 66, pp. 545–549, 1998.

[12] V. Brusic *et al.*, “Copper Corrosion With and Without Inhibitors,” *J Electrochem Soc*, vol. 138, no. 8, p. 2253, 1991.

[13] Y. S. Tan, M. P. Srinivasan, S. O. Pehkonen, and S. Y. M. Chooi, “Self-assembled organic thin films on electroplated copper for prevention of corrosion,” *Journal of Vacuum Science & Technology A: Vacuum, Surfaces, and Films*, vol. 22, no. 4, pp. 1917–1925, Jul. 2004, doi: 10.1116/1.1763901.

[14] M. M. Antonijević, S. M. Milić, and M. B. Petrović, “Films formed on copper surface in chloride media in the presence of azoles,” *Corros Sci*, vol. 51, no. 6, pp. 1228–1237, Jun. 2009, doi: 10.1016/j.corsci.2009.03.026.

[15] M. B. P. Mihajlović and M. M. Antonijević, “Copper Corrosion Inhibitors. Period 2008-2014. A Review,” *Int. J. Electrochem. Sci*, vol. 10, pp. 1027–1053, 2015, [Online]. Available: www.electrochemsci.org

[16] A. Fateh, M. Aliofkhazraei, and A. R. Rezvanian, “Review of corrosive environments for copper and its corrosion inhibitors,” *Arabian Journal of Chemistry*, vol. 13, no. 1, pp. 481–544, Jan. 2020, doi: 10.1016/j.arabjc.2017.05.021.

[17] R. Gašparac, C. R. Martin, E. Stupnišek-Lisac, and Z. Mandic, “In Situ and Ex Situ Studies of Imidazole and Its Derivatives as Copper Corrosion Inhibitors II. AC Impedance, XPS, and SIMS Studies,” *J Electrochem Soc*, vol. 147, no. 3, pp. 991–998, 2000.

[18] H. A. Mohamed, A. A. Farag, and B. M. Badran, “Friendly to environment heterocyclic adducts as corrosion inhibitors for steel in water-borne paints,” *J Appl Polym Sci*, vol. 117, no. 3, pp. 1270–1278, Aug. 2010, doi: 10.1002/app.31838.

[19] A. C. Balaskas, M. Curioni, and G. E. Thompson, “Effectiveness of 2-mercaptobenzothiazole, 8-hydroxyquinoline and benzotriazole as corrosion inhibitors on AA 2024-T3 assessed by electrochemical methods,” *Surface and Interface Analysis*, vol. 47, no. 11, pp. 1029–1039, Nov. 2015, doi: 10.1002/sia.5810.

[20] S. B. Sharma, V. Maurice, L. H. Klein, and P. Marcus, “Local Inhibition by 2-mercaptobenzothiazole of Early Stage Intergranular Corrosion of Copper,” *J Electrochem Soc*, vol. 167, no. 16, p. 161504, Dec. 2020, doi: 10.1149/1945-7111/abcc36.

[21] J. P. Chesick and J. Donohue, “The molecular and crystal structure of 2-mercaptobenzothiazole,” *Acta Crystallogr B*, vol. 27, no. 7, pp. 1441–1444, Jul. 1971, doi: 10.1107/s0567740871004102.

[22] X. Wu, F. Wiame, V. Maurice, and P. Marcus, “Effects of water vapour on 2-mercaptobenzothiazole corrosion inhibitor films deposited on copper,” *Corros Sci*, vol. 189, Aug. 2021, doi: 10.1016/j.corsci.2021.109565.

[23] X. Wu, F. Wiame, V. Maurice, and P. Marcus, “Molecular scale insights into interaction mechanisms between organic inhibitor film and copper,” *Npj Mater Degrad*, vol. 5, no. 1, Dec. 2021, doi: 10.1038/s41529-021-00168-3.

[24] X. Wu, F. Wiame, V. Maurice, and P. Marcus, “2-Mercaptobenzothiazole corrosion inhibitor deposited at ultra-low pressure on model copper surfaces,” *Corros Sci*, vol. 166, Apr. 2020, doi: 10.1016/j.corsci.2020.108464.

[25] M. Finšgar and D. Kek Merl, “An electrochemical, long-term immersion, and XPS study of 2-mercaptobenzothiazole as a copper corrosion inhibitor in chloride solution,” *Corros Sci*, vol. 83, pp. 164–175, 2014, doi: 10.1016/j.corsci.2014.02.016.

[26] X. Wu, F. Wiame, V. Maurice, and P. Marcus, “Adsorption and thermal stability of 2-mercaptobenzothiazole corrosion inhibitor on metallic and pre-oxidized Cu(1 1 1) model surfaces,” *Appl Surf Sci*, vol. 508, Apr. 2020, doi: 10.1016/j.apsusc.2019.145132.

[27] R. Woods, G. A. Hope, and K. Watling, “A SERS spectroelectrochemical investigation of the interaction of 2-mercaptobenzothiazole with copper, silver and gold surfaces,” *J Appl Electrochem*, vol. 30, no. 11, pp. 1209–1222, 2000.

[28] E. Vernack *et al.*, “ToF-SIMS, XPS and DFT study of the adsorption of 2-mercaptobenzothiazole on copper in neutral aqueous solution and corrosion protection in chloride solution,” *Corros Sci*, vol. 210, p. 110854, Jan. 2023, doi: 10.1016/j.corsci.2022.110854.

[29] F. Chiter, D. Costa, V. Maurice, and P. Marcus, “DFT investigation of 2-mercaptobenzothiazole adsorption on model oxidized copper surfaces and relationship with corrosion inhibition,” *Appl Surf Sci*, vol. 537, Jan. 2021, doi: 10.1016/j.apsusc.2020.147802.

[30] F. Chiter, D. Costa, V. Maurice, and P. Marcus, “Chemical interaction, self-ordering and corrosion inhibition properties of 2-mercaptobenzothiazole monolayers: DFT atomistic modelling on metallic copper,” *Corros Sci*, p. 110658, Dec. 2022, doi: 10.1016/j.corsci.2022.110658.

[31] F. Chiter, D. Costa, V. Maurice, and P. Marcus, “Corrosion inhibition of locally de-passivated surfaces by DFT study of 2-mercaptobenzothiazole on copper,” *Npj Mater Degrad*, vol. 5, no. 1, Dec. 2021, doi: 10.1038/s41529-021-00198-x.

[32] X. Wu, F. Wiame, V. Maurice, and P. Marcus, “Moiré Structure of the 2-Mercaptobenzothiazole Corrosion Inhibitor Adsorbed on a (111)-Oriented Copper Surface,” *Journal of Physical Chemistry C*, vol. 124, no. 29, pp. 15995–16001, Jul. 2020, doi: 10.1021/acs.jpcc.0c04083.

[33] M. Bettayeb, V. Maurice, L. H. Klein, L. Lapeire, K. Verbeken, and P. Marcus, “Nanoscale Intergranular Corrosion and Relation with Grain Boundary Character as Studied In Situ on Copper,” *J Electrochem Soc*, vol. 165, no. 11, pp. C835–C841, 2018, doi: 10.1149/2.1341811jes.

[34] H. Chen *et al.*, “Grain boundary passivation studied by in situ scanning tunneling microscopy on microcrystalline copper,” *Journal of Solid State Electrochemistry*, vol. 19, no. 12, pp. 3501–3509, Feb. 2015, doi: 10.1007/s10008-015-2787-x.

[35] S. Mirhashemihaghighi *et al.*, “Electrochemical and Surface Analysis of the Corrosion Protection of Copper by Nanometer-Thick Alumina Coatings Prepared by Atomic Layer Deposition,” *J Electrochem Soc*, vol. 162, no. 8, pp. C377–C384, 2015, doi: 10.1149/2.0081508jes.

[36] J. Kunze, V. Maurice, L. H. Klein, H. H. Strehblow, and P. Marcus, “In situ STM study of the duplex passive films formed on Cu(111) and Cu(001) in 0.1 M NaOH,” *Corros Sci*, vol. 46, no. 1, pp. 245–264, 2004, doi: 10.1016/S0010-938X(03)00140-9.

[37] J. H. Scofield, “Hartree-Slater Subshell Photoionization cross-sections at 1254 and 1487 eV,” *J Electron Spectros Relat Phenomena*, vol. 8, no. 2, pp. 129–137, 1976.

[38] H. Shinotsuka, S. Tanuma, and C. J. Powell, “Calculations of electron inelastic mean free paths. XIII. Data for 14 organic compounds and water over the 50 eV to 200 keV range with the relativistic full Penn algorithm,” *Surface and Interface Analysis*, vol. 54, no. 5, pp. 534–560, May 2022, doi: 10.1002/sia.7064.

[39] L. P. Kazansky, I. A. Selyaninov, and Y. I. Kuznetsov, “Adsorption of 2-mercaptobenzothiazole on copper surface from phosphate solutions,” *Appl Surf Sci*, vol. 258, no. 18, pp. 6807–6813, Jul. 2012, doi: 10.1016/j.apsusc.2012.03.097.

[40] I. A. Arkhipushkin, Yu. E. Pronin, S. S. Vesely, and L. P. Kazansky, “Electrochemical and XPS study of 2-mercaptobenzothiazole nanolayers on zinc and copper surface,” *International Journal of Corrosion and Scale Inhibition*, vol. 3, no. 2, pp. 078–088, 2014, doi: 10.17675/2305-6894-2014-3-2-078-088.

[41] A. Galtayries and J. -P Bonnelle, “XPS and ISS studies on the interaction of H2S with polycrystalline Cu, Cu2O and CuO surfaces,” *Surface and Interface Analysis*, vol. 23, no. 3, pp. 171–179, 1995, doi: 10.1002/sia.740230308.

[42] G. Deroubaix and P. Marcus, “X-ray photoelectron spectroscopy analysis of copper and zinc oxides and sulphides,” *Surface and Interface Analysis*, vol. 18, no. 1, pp. 39–46, 1992, doi: 10.1002/sia.740180107.

[43] M. Finšgar, “EQCM and XPS analysis of 1,2,4-triazole and 3-amino-1,2,4-triazole as copper corrosion inhibitors in chloride solution,” *Corros Sci*, vol. 77, pp. 350–359, Dec. 2013, doi: 10.1016/j.corsci.2013.08.026.

[44] J. F. Moulder, W. F. Stickle, P. E. ’ Sobol, K. D. Bomben, and J. Chastain, “Handbook of X-ray Photoelectron Spectroscopy: A Reference Book of Standard Spectra for Identification and Interpretation of XPS Data,” *Eden Prairie, Minnesota: Physical Electronics Division, PerNin-Elmer Corporation*, vol. 261, 1992.

[45] F. Wiame *et al.*, “Oxidation of α-brass: A photoelectron spectroscopy study,” *Surf Sci*, vol. 641, pp. 51–59, May 2015, doi: 10.1016/j.susc.2015.05.013.